Experimental evidence for two-dimensional states localized in subsurface region of Ge(111)

Koichiro Yaji[a,b,*], Yoshiyuki Ohtsubo[b,c], Shinichiro Hatta[d,b], Hiroshi Okuyama[d], Ryu Yukawa[a], Iwao Matsuda[a], Patrick Le Fèvre[c], François Bertran[c], Amina Taleb-Ibrahimi[c], Akito Kakizaki[a], Tetsuya Aruga[b,d,**]

[a]*Institute for Solid State Physics, The University of Tokyo, Kashiwashi, Chiba 277-8581, Japan.*
[b]*JST CREST, Saitama, 332-0012, Japan.*
[c]*Synchrotron SOLEIL, L'Orme des Merisiers, Saint-Aubin-BP 48, F-91192 Gif sur Yvette, France*
[d]*Department of Chemistry, Graduate School of Science, Kyoto University, Kyoto 606-8502, Japan*

Abstract

The present study gives experimental evidence of two-dimensional electronic states localized in subsurface layers of a Ge(111) substrate, in which a monolayer Pb adsorbed Ge(111) surface is used as a template. We observed three pairs of the subsurface states by angle-resolved photoelectron spectroscopy, which are closely related to bulk heavy-hole, light-hole and spin-orbit split-off bands of Ge(111). The heavy-hole- and light-hole-derived bands show the Rashba-type band crossing at the $\bar{\Gamma}$ point. A density functional theory calculation suggests that the branches of these bands exhibit the Rashba-type spin splitting. On the other hand, we observed peculiar spin polarization for the subsurface states attributed to the bulk spin-orbit split-

---

[*] Corresponding authors
[**] Corresponding authors

Email addresses: `yaji@issp.u-tokyo.ac.jp` (Koichiro Yaji), `aruga@kuchem.kyoto-u.ac.jp` (Tetsuya Aruga)

off band by spin- and angle-resolved photoelectron spectroscopy, where spin polarization of each branch is inverted with respect to $\bar{\Gamma}$ and the degeneracy, expected for a normal Rashba spin-split surface state is lifted at $\bar{\Gamma}$.

Key words: Rashba effect, Semiconductor, Surface state, Angle-resolved photoelectron spectroscopy, Spin-resolved photoelectron spectroscopy

PACS: 73.20.Fz, 71.70.Ej, 79.60.?i

1. Introduction

One of the steps in developing spintronic applications is to yield a spin-polarized electron in a semiconductor. For this aim, the Rashba-type spin-orbit interaction has a great potential. The inversion symmetry is broken at the surface or interface. According to the framework of the Rashba effect, the spin degeneracy is then lifted by the potential gradient in the surface normal direction and an electronic state is split into two in the momentum space, where the spin orientation is perpendicular to both the surface normal and the momentum of the electron [1, 2]. Solid surface systems have been offering an opportunity to study the Rashba effect by angle-resolved photoelectron spectroscopy (ARPES) and spin- and angle-resolved photoelectron spectroscopy (SARPES) so far. Here, we notice that the Rashba spin-polarized bands were mainly reported on the surfaces including heavy element atoms, such as Au [3, 4], Bi [5], and a monolayer of heavy-element atoms adsorbed on light-element substrate [6, 7, 8, 9, 10].

On the other hand, recently, a new type of spin-polarized surface states derived from Ge, a lighter element, was found on Bi/Ge(111), Br/Ge(111), Tl/Ge(111) and Pb/Ge(111), in which the surface states disperse near the valence band maximum (VBM) of Ge bulk bands [11, 12, 13, 14, 15]. An insight into the spin-polarized two-dimensional states has been provided by a density functional theory (DFT) calculation [13]. Layer-resolved charge density analysis suggests that maximum of the charge density is located between the fifth and tenth Ge layers and the charge density gradually decays into the bulk. The spin-polarized states may therefore be classified as "subsurface states". The formation of the subsurface states is explained with the bulk electronic states modified by the truncation of a bulk periodicity at the surface, suggesting that the subsurface states originate from bulk heavy-hole, light-hole, and spin-orbit split-off bands of Ge. The spin polarization of the subsurface states is due to the Rashba effect and the size of the spin-split energy is determined by the atomic spin-orbit interaction in a Ge atom. On the other hand, experimentally, details of the energy dispersion of the subsurface states remain unclear. For instance, it is difficult to identify the energy dispersion of light-hole-derived states as well as the spin splitting of heavy-hole-derived states [11, 12]. We consider that low photoelectron intensities from the subsurface states and the presence of the Ge bulk bands hinder the clear identification of the band structures of the subsurface states near VBM. In addition, the charge density analysis suggests that the subsurface states have a charge-density modulation along the surface normal while the subsurface states are intrinsic two-dimensional states. Such modulation may yield a pseudo-dispersion of the subsurface-state bands along a k_z direction. Photon energy dependence of ARPES are thus required for clarifying the energy dispersion along the k_z direction.

In the present study, we experimentally clarify the electronic band structure of the subsurface states near VBM of the Ge(111) substrate covered with a monolayer Pb (Pb/Ge(111)-β). High-resolution ARPES with a He lamp provides the detail of the energy dispersion of the subsurface states. In an ARPES experiment with synchrotron radiation, several photon energies were selected in order to examine whether or not the subsurface states exhibit the energy dispersion along the k_z direction. The result gives direct evidence that the subsurface states are surely two-dimensional. From SARPES, we confirmed that one of the subsurface states shows peculiar spin structure, which is against the conventional picture of the Rashba-type band crossing. The DFT calculation supports the assignment of the experimental band structure. The present results provide experimentally significant and conclusive information on the subsurface states on Ge(111) induced by the bulk truncation.

2. Experimental methods

Experiments were performed in ultrahigh-vacuum systems with base pressures lower than 2.0×10^{-8} Pa. In the ARPES experiment with monochromatic He I ($h\nu$ = 21.2 eV) radiation, we used an angular mode of a hemispherical electron energy analyzer (VG SCIENTA R3000) in Kyoto University. The ARPES measurements with synchrotron radiation were performed with a VG SCIENTA R4000 analyzer at CASSIOPÉE beam line in SOLEIL in France. The SARPES measurements were performed at the beam line 19A of Photon Factory in Japan, using synchrotron radiation and the set of a hemispherical electron energy analyzer (SPECS Phoibos 150) and a very low energy electron diffraction (VLEED) type spin polarimeter [16] with an energy resolution of 160 meV. The effective Sherman function of the spin polarimeter was 0.35.

For all of the experiments, samples were prepared *in situ* in a molecular beam epitaxy chamber connected to each analysis chamber. A Ge(111) substrate was prepared by several cycles of 0.7 keV Ar^+ sputtering at room temperature (RT) and subsequent annealing up to 870 K for a few seconds. The surface cleanliness was checked by a sharp $c(2\times8)$ low-energy electron diffraction (LEED) pattern. Pb was then deposited onto the surface kept at RT from an alumina crucible heated with a tungsten filament. The surface after the Pb deposition was annealed at 570 K for a few minutes to prepare well-ordered wide terraces. Total amount of Pb atoms on the surface was calibrated by checking a photoelectron intensity from a Pb-derived surface-state band, labeled S_{Pb} in Fig. 1(a), of Pb/Ge(111)-β [10, 17]. Note that the photoelectron intensity from S_{Pb} is prominent in the second surface Brillouin zone (SBZ). The reconstructed surface of Pb/Ge(111)-β yielded a sharp $(\sqrt{3}\times\sqrt{3})R30^\circ$ LEED pattern.

Density-functional theory (DFT) calculation has been performed using the WIEN2k computer code based on the augmented plane wave + local orbitals (APW + lo) method including the spin-orbit interaction [18]. We adopted the modified Becke and Johnson (mBJ) potential together with the exchange-correlation potential constructed by using the local density approximation [19, 20]. The surface was modeled by a 44-layer Ge(111) slab with the both sides covered with a $(\sqrt{3}\times\sqrt{3})R30^\circ$-Pb layer. We note that the thick slab is required to reproduce the subsurface states because of the long decay length into the bulk.

3. Results and discussion

Figure 1(a) shows an ARPES intensity map along $\bar{\Gamma}\bar{M}$ in the $(\sqrt{3}\times\sqrt{3})R30^\circ$ SBZ, which coincides with a $[1\bar{1}0]$ axis of Ge(111)-(1×1), measured with photon energy of 21.2 eV from the He lamp. The dashed curves represent the upper edge of the bulk bands obtained from tight-binding calculation with parameters adjusted to the experimental bulk band structure [13]. The bulk bands consist of heavy-hole band, light-hole band, and spin-orbit split-off band at $\bar{\Gamma}$. Here, energy positions of the light-hole and spin-orbit split-off bands interconvert away from $\bar{\Gamma}$ because of the hybridization between these bands. In the present article, the bulk bands are named B_{HH}, B_{LH} and B_{SO} as shown in Fig. 1(a), respectively.

As shown in Fig. 1(a), we observed a pair of metallic bands with the Fermi wave vector of 0.38 Å^{-1}, labeled S_{Pb}. This pair of bands is spin-polarized due to the Rashba effect, which have already been reported in our papers [10, 17]. A nearly flat band observed at $\sim$0.9 eV is also attributed to a Pb-derived band [10, 17]. On the other hand, several bands are found near VBM and disperse downward from $\bar{\Gamma}$. Hereafter, we focus on these bands.

Figure 1(b) exhibits an ARPES intensity map recorded with photon energy of 21.2 eV with high energy resolution along $\bar{\Gamma}\bar{M}$ in the $(\sqrt{3}\times\sqrt{3})R30^\circ$ SBZ near VBM at 30 K. A momentum distribution curve (MDC) at the binding energy of 20 meV is also represented in the lower panel in Fig. 1(b). Schematic drawing of the band structure is represented in Fig. 1(c). We found from Fig. 1(a) that $S_1^{\pm}$ appears in the projected bulk band gap and disperses almost parallel to B_{HH} at larger $k_{\parallel}$ (> 0.15 Å^{-1}). In addition, $S_1^{\pm}$ crosses the Fermi level near $\bar{\Gamma}$. From the high-resolution image and the MDC

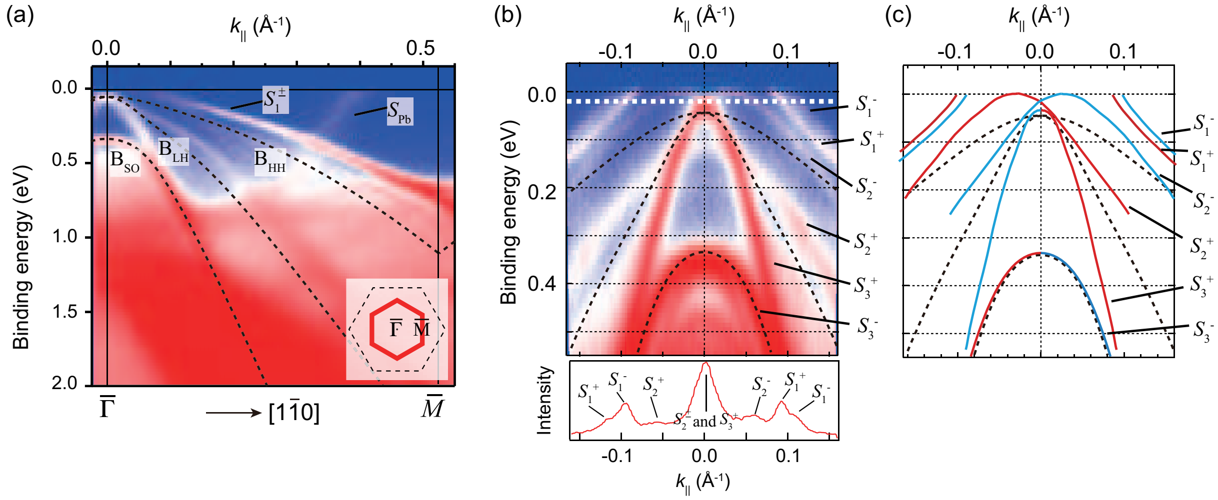

Figure 1: (Color online) ARPES intensity map of Pb/Ge(111)-β along $\bar{\Gamma}\bar{M}$ in the $(\sqrt{3}\times\sqrt{3})R30°$ SBZ with the photon energy of 21.2 eV. The SBZ are shown in the inset, where the dashed (thin) and solid (bold) hexagons denote the (1×1) and $(\sqrt{3}\times\sqrt{3})R30°$ periodicity, respectively. Dashed curves represent the bulk band edges, i.e. bulk heavy-hole (B_{HH}), light-hole (B_{LH}), and spin-orbit split-off (B_{SO}) bands. (b) (*upper panel*) ARPES image recorded with the photon energy of $h\nu = 21.2$ eV with high-energy-resolution near VBM. Dashed curves represent the bulk band edges, B_{HH}, B_{LH} and B_{SO}. (*lower panel*) A momentum distribution curve taken with the photoelectron intensity within a 20 meV energy window centered at the binding energy of 20 meV, shown by a bold dashed line in the upper panel. (c) Schematic drawing of the surface-state bands of $S_1^{\pm}$, $S_2^{\pm}$ and $S_3^{\pm}$. Red and blue curves represent the spin direction toward $[11\bar{2}]$ and $[\bar{1}\bar{1}2]$.

shown in Fig. 1(b), we can recognize that $S_1^{\pm}$ is split into two, labeled S_1^+ and S_1^- for each branch. The Fermi wave vectors k_{F} of S_1^+ (S_1^-) are estimated to be 0.082 $\mathrm{\AA}^{-1}$ (0.100 $\mathrm{\AA}^{-1}$) on a positive $k_{\|}$ and at -0.100 $\mathrm{\AA}^{-1}$ (-0.082 $\mathrm{\AA}^{-1}$) on a negative $k_{\|}$. Also, we found a pair of bands, labeled S_2^+ and S_2^-, dispersing along B_{LH}. The maxima of S_2^+ and S_2^- reach the Fermi level and are symmetrically shifted from $\bar{\Gamma}$ by 0.03 – 0.04 $\mathrm{\AA}^{-1}$. S_2^+ and S_2^- are degenerated at $\bar{\Gamma}$ at binding energy of 30 meV. This implies that a pair of S_2^+ and S_2^- shows the Rashba-type band crossing. For the S_3^+ band, the energy maximum is quite close to the crossing point of S_2^+ and S_2^-. And then, S_3^+ shows the energy dispersion downward from $\bar{\Gamma}$ into the bulk spin-orbit gap. S_3^- disperses along the upper edge of B_{SO} and almost parallel to S_3^+ at $|k_{\|}| > 0.06$ $\mathrm{\AA}^{-1}$.

Figures 2(a)-2(d) show ARPES intensity maps along $\bar{\Gamma}\bar{M}$ in the $(\sqrt{3}\times\sqrt{3})R30^\circ$ SBZ with synchrotron radiation. Here, we selected the several photon energies in order to confirm the energy dispersion along the k_{z} direction with the z axis defined as perpendicular to the surface. We note that the ARPES image obtained with $h\nu = 21$ eV shown in Fig. 2(c) agrees well with the image recorded with the He lamp shown in Fig. 1(a). $S_1^{\pm}$ is observed with photon energies of 17, 21, and 26 eV. In addition, there is no energy shift for $S_1^{\pm}$ depending on the photon energy, meaning that $S_1^{\pm}$ exhibits no energy dispersion along the k_{z} direction. This serves an evidence that $S_1^{\pm}$ is a two-dimensional state. S_2^+ and S_2^- are observed with photon energies of 17, 19 and 21 eV and the energy positions of the bands do not change. Thus, S_2^+ and S_2^- are also assigned as two-dimensional states. S_3^+ and S_3^- appear in all images in Fig. 2. The energy dispersions of S_3^+ and S_3^- are completely identical, indicating that S_3^+ and S_3^- are also two-dimensional states.

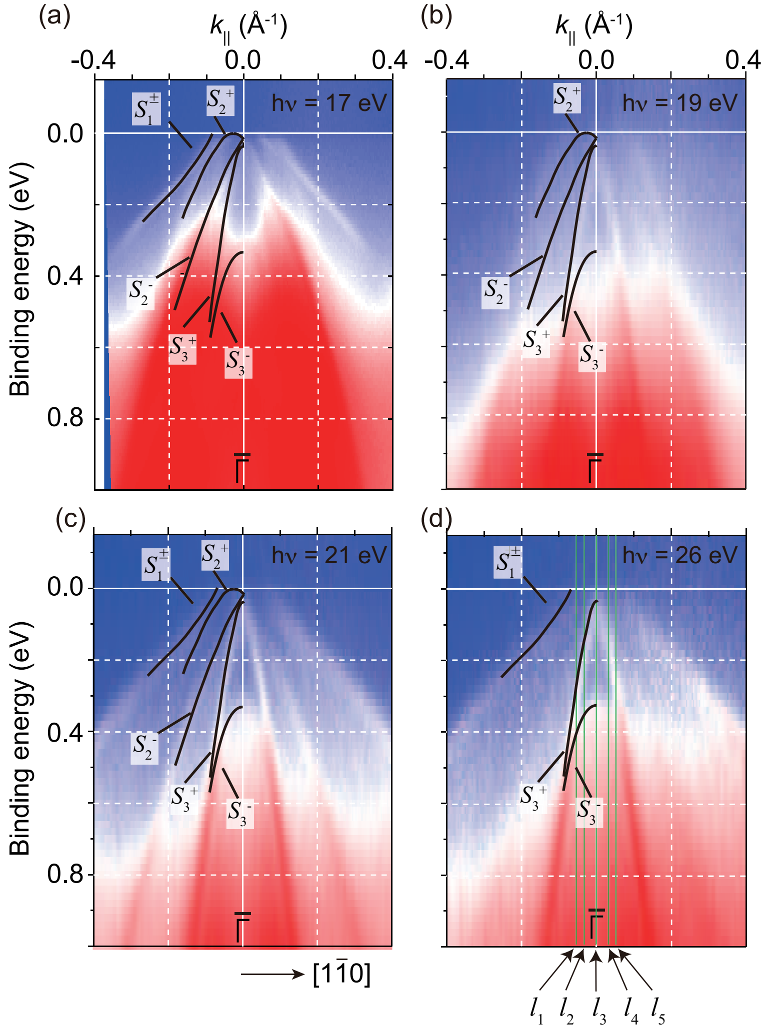

Figure 2: (Color online) (a-d) ARPES images of Pb/Ge(111)-β along $\bar{\Gamma}\bar{M}$ in the $(\sqrt{3}\times\sqrt{3})R30^\circ$ SBZ recorded with the photon energies of $h\nu = 17$ eV, 19 eV, 21eV, 26 eV. Solid curves represent the band structures for guides to the eyes.

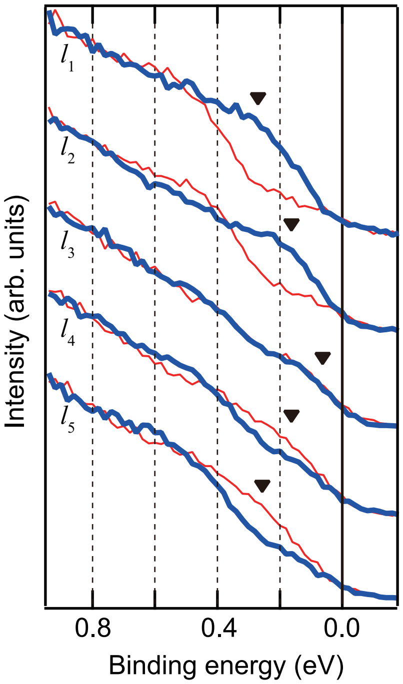

Figure 3: (Color online) (a) Spin- and angle-resolved photoelectron spectra taken with several selected wave vectors, which are shown with thin solid (green) lines in Fig. 2(d). Here, l_1–l_5 correspond to emission angles of -1.3°, 0.8°, 0.0°, 0.7° and 1.2° with respect to the surface normal, respectively. The spin polarization toward $[11\bar{2}]$ and $[\bar{1}\bar{1}2]$ directions is represented with thin (red) and bold (blue), respectively. Triangles denote energy positions of S_3^+ obtained from the ARPES data shown in Fig. 2(d).

Next, we describe the results of SARPES shown in Fig. 3. In SARPES, we focus on the spin polarization of S_3^+ because the branches of S_3^+ and S_3^- are quite different from the conventional Rashba-type band structure, as these bands do not show the band crossing at $\bar{\Gamma}$. The spin-resolved photoelectron spectra were recorded with the photon energy of 26 eV at several selected $k_\parallel$'s, denoted as l_1–l_5 in Fig. 2(d). Here, we have found from the photon energy dependence of ARPES shown in Fig. 2 that S_3^+ is clearly observed with $h\nu = 26$ eV whereas the photoelectron intensity from $S_2^\pm$ is rather weak. Thus, use of the photon energy of 26 eV allows us to predominantly observe the spin-resolved spectra from S_3^+ although S_3^+ is energetically close to $S_2^\pm$ near $\bar{\Gamma}$. The spin polarimeter was arranged to observe the spin polarization toward $[11\bar{2}]$ and $[\bar{1}\bar{1}2]$.

It is found that the spin-resolved spectra along l_3 are almost identical. This indicates that the spin polarization of S_3^+ is zero at $\bar{\Gamma}$. On the other hand, the spin-polarized spectra are observed at l_1, l_2, l_4 and l_5. For the spin-resolved spectra at l_1 and l_2, the spin polarization toward $[\bar{1}\bar{1}2]$ is found and the spin polarization toward $[11\bar{2}]$ is negligible. Here, the peaks for l_1 and l_2 are located at 0.3 eV and 0.2 eV, respectively. The spin-resolved spectra at l_4 and l_5 exhibit the spin polarization toward $[11\bar{2}]$. The peak position of l_4 (l_5) is almost same as l_2 (l_1). The energy dispersion of the spin-resolved spectra agrees well with the ARPES results, where the energy positions of S_3^+ obtained from Fig. 2(d) are represented in Fig. 3. We therefore conclude that S_3^+ shows no spin polarization at $\bar{\Gamma}$ and the spin polarization direction is inverted in the band around $\bar{\Gamma}$. We note that $S_1^\pm$ are not clear at l_1 and l_5 in the SARPES measurements because the photoelectron intensities from

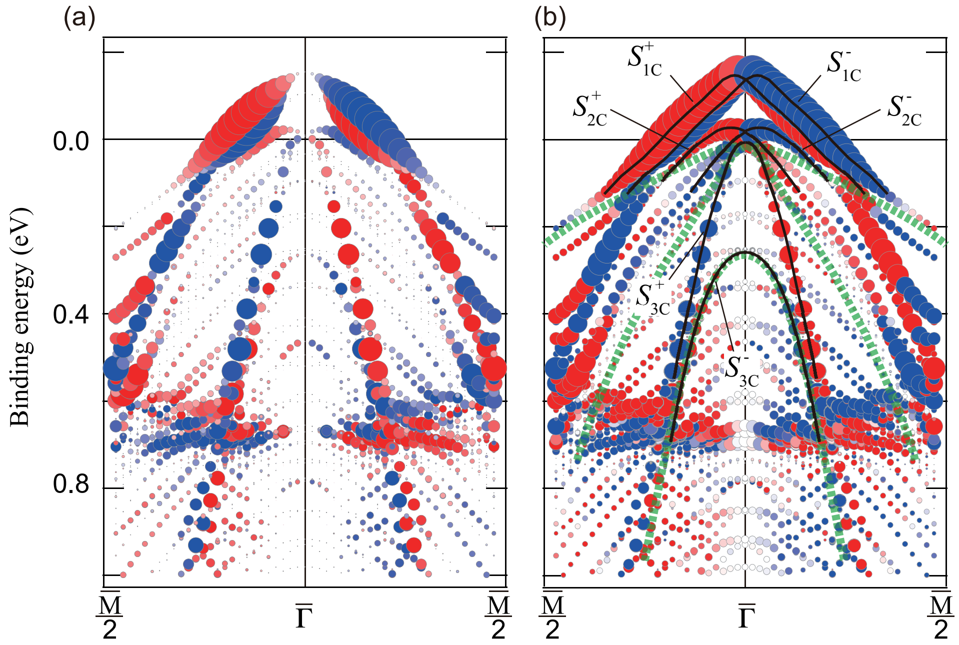

Figure 4: (Color online) Calculated band structure of Pb/Ge(111)-β along $\bar{\Gamma}\bar{M}$ near VBM. Opposite spin orientations are indicated by colors of blue and red (colors, online). In panel (a), the size of the circle is proportional to the net spin polarization ($R^{-}_{k_\parallel,E}$ defined by Eq. (1)). In panel (b), the size of the circle represents the total contribution of Ge atoms in 1st-6th layers ($R^{+}_{k_\parallel,E}$ defined by Eq. (1)). The bold dashed curves represent the bulk band edges of heavy-hole, light-hole, and spin-orbit split-off bands [13]. Thin solid curves represent the band structure of the subsurface states.

$S_1^{\pm}$ are weak.

We performed a DFT calculation in order to obtain further information on the spin structure of the subsurface states of Pb/Ge(111)-β. Figures 4(a) and (b) show the calculated band structures for Pb/Ge(111)-β along $\bar{\Gamma}\bar{M}$ in the $(\sqrt{3}\times\sqrt{3})R30^\circ$. The sizes of the circles are given by

$$R^{\pm}_{k_\parallel,E} \propto \left| \sum_{i=0}^{n} \left(|\langle \phi^i, \uparrow | \mathbf{\Psi}_{k_\parallel,E}\rangle|^2 \pm |\langle \phi^i, \downarrow | \mathbf{\Psi}_{k_\parallel,E}\rangle|^2 \right) \right|, \tag{1}$$

where $|\phi^i, \uparrow\rangle$ and $|\phi^i, \downarrow\rangle$ denote atomic orbitals in ith layers with spin polarization, and $|\boldsymbol{\Psi}_{k_\parallel,E}\rangle$ is an eigenfunction of a calculated state at $(k_\parallel, E)$. The summation of the atomic orbitals from 1st to 6th layers was carried out. The zeroth layer corresponds to the Pb layer at the surface and the 1st layer corresponds to the topmost layer of the Ge substrate. Thus, $R^-_{k_\parallel,E}$ expresses the net spin polarization of the Ge atoms. The calculated band structure with $R^-_{k_\parallel,E}$ is represented in Fig. 4(a), in which the size of the circle represents the amplitude of the spin polarization and colors of the circles give the spin directions. We notice that small spin polarization makes difficulty in clear identification of the band structure, especially in the proximity to $\bar{\Gamma}$. In order to make clear the band structure, we also provide another panel drawn with $R^+_{k_\parallel,E}$ in Fig. 4(b). $R^+_{k_\parallel,E}$ represents the total contribution from the Ge atoms in the surface and subsurface layers. This indicates that the size of the circle is proportional to the partial charge of the Ge atoms. We note that Pb 6p orbitals have a negligible contribution near VBM [10, 17].

S^+_{1C} and S^-_{1C} exhibit the energy dispersion along the edge of the bulk heavy-hole states in the projected bulk band gap and cross the Fermi level. The band structure of S^+_{1C} and S^-_{1C} below the Fermi level is in agreement with the ARPES result shown in Fig. 1(b). Also, the calculated band structure suggests that a pair of $S^\pm_{1C}$ shows the spin splitting around $\bar{\Gamma}$, in particular the spin polarization is prominent near the Fermi level. The spin polarization direction of one branch is opposite to another branch. On the other hand, the branches of $S^\pm_{1C}$ are degenerated at $\bar{\Gamma}$ above the Fermi level and the spin polarization is zero at $\bar{\Gamma}$. Thus, the spin splitting of $S^\pm_{1C}$ is due to the Rashba effect. The amplitude of the spin splitting for $S^\pm_{1C}$ is 27 meV at the

Fermi wave vector. Note that the spin splitting of $S_{1C}^{\pm}$ was not detected by SARPES because the size of the spin splitting is rather small compared with the energy resolution of SARPES.

The energy dispersions of S_{2C}^{+} and S_{2C}^{-} are also in agreement with ARPES. The branches of $S_{2C}^{\pm}$ are degenerate at $\bar{\Gamma}$ near the Fermi level and are spin-polarized around $\bar{\Gamma}$ toward opposite directions. This behavior agrees with the Rashba-type spin splitting. The spin polarization of $S_{2C}^{\pm}$ is moderate in the projected bulk band gap compared with $S_{1C}^{\pm}$. The spin polarization is however weakened at $|k_{\parallel}| > 0.1$ Å^{-1} because the branches of $S_{2C}^{\pm}$ merge into the Ge bulk bands.

S_{3C}^{+} and S_{3C}^{-} also appear in the calculated band images, which is consistent with the ARPES results. The energy maximum of S_{3C}^{+} nearly reaches to the crossing point of $S_{2C}^{\pm}$ at $\bar{\Gamma}$ and S_{3C}^{+} shows the energy dispersion downward from $\bar{\Gamma}$. The spin polarization of S_{3C}^{+} is negligible at $\bar{\Gamma}$ while it is enhanced around $\bar{\Gamma}$. The spin polarization direction is inverted with respect to $\bar{\Gamma}$. Concerning S_{3C}^{-}, the energy maximum is located at $\bar{\Gamma}$ at the binding energy of 250 meV and the band disperses downward from $\bar{\Gamma}$. The spin polarization of S_{3C}^{-} is inverted with respect to $\bar{\Gamma}$ and is opposite to that of S_{3C}^{+}. However, the amplitude of the spin polarization of S_{3C}^{-} is much smaller than that of S_{3C}^{+}. We notice that S_{3C}^{-} disperses along the edge of the bulk spin-orbit split-off band, meaning that the electrons in the S_{3}^{-} band can merge into the bulk bands. This reduces the spin polarization of S_{3C}^{-}, which is consistent with the fact that the spin polarization of S_{3}^{-} was not clearly observed by SARPES.

We have experimentally clarified the band structures of the subsurface states of Pb/Ge(111)-β. We consider that a scenario of the formation of the subsurface states is common with the other systems such as Bi/Ge(111), Br/Ge(111), Tl/Ge(111) [11, 12, 13]. The subsurface states are yielded from the bulk electronic states perturbed by the truncation of bulk periodicity at the surface. In principle, the subsurface states of Pb/Ge(111)-β are thus attributed to the B_{HH}, B_{LH} and B_{SO} bands. The energy position of each subsurface state depends on a type of the bulk truncation, meaning that the energy of the subsurface states can be modified by ad-layers. In fact, the light-hole-derived $S_2^{\pm}$ bands of Pb/Ge(111)-β appear in the projected bulk band gap near $\bar{\Gamma}$ while the light-hole-derived bands for Bi/Ge(111) and Br/Ge(111) were found in the bulk bands, for example.

From the ARPES results, we found that the spin splitting of $S_1^{\pm}$ is 30 meV at $k_F = 0.1$ Å^{-1}. The Rashba parameter of $S_1^{\pm}$ is thus estimated to be 0.15 eV Å. On the other hand, it is difficult to accurately estimate the Rashba parameter for the pair of $S_2^{\pm}$ only from the ARPES results because the topmost part of the branches is above the Fermi level and the large intensity from S_3^{+} hinders us locating the peak positions of $S_2^{\pm}$ around $\bar{\Gamma}$. We thus evaluate the Rashba parameter of $S_{2C}^{\pm}$ from the calculated band structure shown in Fig. 4. The energy maxima of $S_{2C}^{\pm}$ are located at $|k_{\parallel}| = \pm 0.04$ Å^{-1}. The size of the spin splitting of $S_{2C}^{\pm}$ is then estimated to be 0.034 eV at 0.04 Å^{-1}, which yields the Rashba parameter of about 0.4 eV Å. The sizes of the spin splitting of $S_1^{\pm}$ and $S_2^{\pm}$ are consistent with that of the atomic spin-orbit splitting of Ge 4p [21].

Finally, we describe the peculiar band $S_3^{\pm}$, which is quite different from the conventional Rashba-type band crossing. The energetic order between the bulk light-hole and spin-orbit split-off bands is inverted around $\bar{\Gamma}$ because of the spin-orbit interaction of Ge, which makes a finite spin-orbit energy gap. One spin-polarized branch S_3^+ disperses across the spin-orbit gap. This manner is similar to the case of the spin-polarized surface states on topological insulators (TI). TI has a bulk band gap which opens due to the spin-orbit interaction and the topological surface states disperse continuously across the bulk spin-orbit gap. In addition, $S_3^\pm$ are surface resonances. The surface resonances can switch its partner to an arbitrary band at high-symmetry point because of the large contribution from the bulk states. Thanks to this, Kramars degeneracy of $S_3^\pm$ at $\bar{\Gamma}$ is preserved even without the Rashba-type band crossing. This situation yields the spin-polarized S_3^+ and its counterpart S_3^-. Similar band structures are also found in Bi/Ge(111), Br/Ge(111), Tl/Ge(111). The formation mechanism of $S_3^\pm$ has been discussed in the former paper in detail [13].

4. Summary

In summary, we have investigated the two-dimensional states localized in subsurface regions of Pb/Ge(111)-β near VBM by ARPES, SARPES and the DFT calculation. From the high-resolution ARPES, the energy dispersions of the subsurface states were experimentally identified. Photon energy dependence of ARPES using synchrotron radiation clarified that the subsurface states exhibit two-dimensional nature. The spin polarization of the subsurface states was confirmed by SARPES and the DFT calculation. The spin polarization of $S_1^\pm$ and $S_2^\pm$ is explained by the conventional Rashba effect while $S_3^\pm$ exhibit peculiar spin-polarized band structures.

5. Acknowledgments

The authors thank J. Pinon, D. Ragonnet, and M. D′Angelo for their support during the experiments at the CASSIOPÉE beam line in synchrotron SOLEIL. The present work was financially supported by Bilateral Joint Research Project between Japan (JSPS) and France (CNRS) and the JSPS Grant-in-Aid for Young Scientists (B), Grant No. 24740197.

References

[1] E. I. Rashba, Sov. Phys. Solid State 2 (1960) 1109.

[2] Y. A. Bychkov and E. I. Rashba, JETP Lett. 39 (1984) 78.

[3] S. LaShell, B. A. McDougall, and E. Jensen, Phys. Rev. Lett. 77 (1996) 3419.

[4] M. Hoesch, M. Muntwiler, V. N. Petrov, M. Hengsberger, L. Patthey, M. Shi, M. Falub, T. Greber, and J. Osterwalder, Phys. Rev. B 69 (2004) 241401(R).

[5] Yu. M. Koroteev, G. Bihlmayer, J. E. Gayone, E.V. Chulkov, S. Blügel, P.M. Echenique, and Ph. Hofmann Phys. Rev. Lett. 93 (2004) 046403.

[6] T. Nakagawa, O. Ohgami, Y. Saito, H. Okuyama, M. Nishijima, and T. Aruga, Phys. Rev. B 75 (2007) 155409.

[7] C. R. Ast, J. Henk, A. Ernst, L. Moreschini, M. C. Falub, D. Pacilé, P. Bruno, K. Kern, and M. Grioni, Phys. Rev. Lett. 98 (2007) 186807.

[8] I. Gierz, T. Suzuki, E. Frantzeskakis, S. Pons, S. Ostanin, A. Ernst, J. Henk, M. Grioni, K. Kern, and C. R. Ast, Phys. Rev. Lett. 103 (2009) 046803.

[9] S. Hatta, T. Aruga, Y. Ohtsubo, and H. Okuyama, Phys. Rev. B 80 (2009) 113309.

[10] K. Yaji, Y. Ohtsubo, S. Hatta, H. Okuyama, K. Miyamoto, T. Okuda, A. Kimura, H. Namatame, M. Taniguchi, and T. Aruga, Nature Commun. 1 (2010) 17.

[11] Y. Ohtsubo, S. Hatta, K. Yaji, H. Okuyama, K. Miyamoto, T. Okuda, A. Kimura, H. Namatame, M. Taniguchi, and T. Aruga, Phys. Rev. B 82 (2010) 201307(R).

[12] Y. Ohtsubo, S. Hatta, N. Kawai, A. Mori, Y. Takeichi, K. Yaji, H. Okuyama, and T. Aruga, Phys. Rev. B 86 (2012) 165325.

[13] Y. Ohtsubo, K. Yaji, S. Hatta, H. Okuyama, and T. Aruga, Phys. Rev. B 88 (2013) 245310.

[14] S.-J. Tang, T.-R. Chang, C.-C. Huang, C.-Y. Lee, C.-M. Cheng, K.-D. Tsuei, H.-T. Jeng, and C.-Y. Mou, Phys. Rev. B 81 (2010) 245406.

[15] C.-H. Lin, T.-R. Chang, R.-Y. Liu, C.-M. Cheng, K.-D. Tsuei, H.-T. Jeng, C.-Y. Mou, I. Matsuda, and S.-J. Tang, New J. Phys. 16 (2014) 045003.

[16] T. Okuda, Y. Takeichi, Y. Maeda, A. Harasawa, I. Matsuda, T. Kinoshita, and A. Kakizaki, Rev. Sci. Instrum. 79 (2008) 123117.

[17] K. Yaji, S. Hatta, T. Aruga, and H. Okuyama, Phys. Rev. B 86 (2012) 235317.

[18] P. Blaha, K. Schwarz, G. Madsen, D. Kvasnicka, and J. Luitz, WIEN2k: An Augmented PlaneWave + Local Orbitals Program for Calculating Crystal Properties (Karlheinz Schwarz, Techn. Universitt Wien, Wien, 2001).

[19] A. D. Becke and E. R. Johnson, J. Chem. Phys. 124 (2006) 221101.

[20] F. Tran and P. Blaha, Phys. Rev. Lett. 102 (2009) 226401.

[21] S. Kotochigova, Z. H. Levine, E. L. Shirley, M. D. Stiles, and C. W. Clark, Phys. Rev. A 55 (1997) 191.